Active control of radiation beaming from Tamm nanostructures by optical microscopy

Fu Feng, Clémentine Symonds, Catherine Schwob, Joël Bellessa, Agnès Maitre, Jean-Paul Hugonin, Laurent Coolen

New Journal of Physics
The open access journal at the forefront of physics

Deutsche Physikalische Gesellschaft DPG IOP Institute of Physics

PAPER • OPEN ACCESS

Active control of radiation beaming from Tamm nanostructures by optical microscopy

To cite this article: Fu Feng *et al* 2018 *New J. Phys.* **20** 033020

New Journal of Physics
The open access journal at the forefront of physics

Deutsche Physikalische Gesellschaft DPG
IOP Institute of Physics

Published in partnership with: Deutsche Physikalische Gesellschaft and the Institute of Physics

OPEN ACCESS

RECEIVED
21 December 2017

REVISED
9 February 2018

ACCEPTED FOR PUBLICATION
15 February 2018

PUBLISHED
28 March 2018

PAPER

Active control of radiation beaming from Tamm nanostructures by optical microscopy

Fu Feng[1], Clémentine Symonds[2], Catherine Schwob[1], Joël Bellessa[2], Agnès Maître[1], Jean-Paul Hugonin[3] and Laurent Coolen[1,4]

[1] Sorbonne Universités, UPMC Univ Paris 06, CNRS-UMR 7588, Institut des NanoSciences de Paris, F-75005, Paris, France
[2] Institut Lumière Matière, Université de Lyon, UMR5306 Université Lyon 1-CNRS, F-69622 Villeurbanne, France
[3] Laboratoire Charles Fabry, Institut d'Optique, CNRS, Univ Paris-Sud, 2 avenue Fresnel, F-91127 Palaiseau cedex, France
[4] Author to whom any correspondence should be addressed.

E-mail: laurent.coolen@insp.jussieu.fr

Keywords: optical Tamm structure, nanocrystals, emission pattern control

Supplementary material for this article is available online

Abstract

Active control of the radiation orientation (beaming) of a metallic antenna has been reported by various methods, where the antenna excitation position was tuned with a typical 50 nm precision by a near-field tip or an electron-beam. Here we use optical microscopy to excite and analyze the fluorescence of a layer of nanocrystals embedded in an optical Tamm state nanostructure (metallic disk on top of a Bragg mirror). We show that the radiation pattern can be controlled by changing the excitation spot on the disk with only micrometer precision, in a manner which can be well described by numerical simulations. A simplified analytical model suggests that the propagation length of the in-plane confined optical modes is a key parameter for beaming control.

Nanophotonic structures such as optical cavities or nano-antennas provide exciting opportunities for manipulating light emission [1]. Controlling the emission orientation (beaming) is one of the challenges for such structures. For cavities in photonic crystals, the position of the holes can be tuned to focus the emission in a cone of $\pm 20°$–$30°$ around the optical axis [2–4]. For a periodic plasmonic surface, the radiation angle can be chosen through the period [5, 6]. For Yagi-Uda antennas, the emission can be directed forward at angle $\theta = +50°$ with very low backwards ($-50°$) radiation [7]. It is then the design of the nanostructure which determines the direction of radiation.

Some nanostructures can radiate with different orientations depending on the position, inside these structures, of the source dipole which excites their electromagnetic mode. For a patch antenna, the measured emission was tilted from normal by 5° due to an off-centering of the emitter by 15 nm [8]. For a metallic cylinder [9], hole [10] or ring resonator [11] of diameter ~100 nm or for a row of cylinders [12] studied by cathodoluminescence, the emission cone can be oriented to the left or to the right by changing the position of the excitation electron beam. A similar beaming of the emitted light has also been shown by tuning the position of the tip of a scanning tunneling microscope used to electrically excite a gold triangular nanoparticle [13]. An active control of the beaming was thus provided by use of a near-field probe. Moreover, this effect may allow to tune the radiation pattern by choosing the position of a fluorescent emitter (for instance a single-photon source) deposited inside or near the nanostructure. However, for the antennas considered so far in [9–13], a control of the position of the order of 50 nm is required, which was achieved either by near-field [13] or electron-beam excitation [9–12]. For the patch antenna [8], 25 nm precision positioning in optical lithography has been achieved by very fine *in situ* optical lithography [14].

In this paper, we analyze the effect of the source position on the radiation pattern for nanostructures of confined Tamm states. Optical Tamm states (sometimes called Tamm plasmons) are electromagnetic states confined along the plane between a Bragg mirror and a metallic layer [15, 16] (we will refer to these states as '2D-Tamm'). They allow versatile fabrication of confined Tamm structures (here called '0D-Tamm') by deposition

of a metallic disk on a Bragg mirror [17], which can be used to enhance fluorescence [18], single-photon emission [19] or laser effects [20], with polarization control through the structure's shape [21]. By selective optical excitation of a given position in a layer of emitters in the 0D-Tamm structure, we show here that the position of the source can be used to tune the radiation pattern asymmetry. Unlike the antennas discussed above, for Tamm structures the level of position control required is of the order of 1 μm, so that active control of the emission pattern is obtained by optical microscopy rather than near-field methods. Moreover, fabrication of a structure with controlled emission pattern asymmetry could be obtained by positioning a single emitter with standard optical lithography, with only 1 μm resolution required. Our experimental results are found in good agreement with numerical simulations, so that the use of such structures for controlled beaming can be simulated *a priori*. A simple analytical model suggests that a key parameter for beaming control is the propagation length of the electromagnetic modes in the nanostructure.

The localized Tamm states structures fabrication was described in [22, 23] and is briefly summarized here: a TiO_2/SiO_2 $\lambda/4$ Bragg mirror was fabricated with stop band centered at 640 nm (7 pairs, SiO_2 index 1.44, TiO_2 index 2.25, maximum reflectivity 98%, manufacturer Kerdry, France). The upper layer was a 80 nm SiO_2 thin film, in order to position the emitters at a height inside the sample where the Tamm-state electric field is maximum. A layer of colloidal CdSe/CdS nanocrystals (CdSe core diameter 3 nm, CdS shell thickness 12 nm, emission centered at 640 nm) was then deposited on top of the Bragg mirror with an estimated density of 6000 μm^{-2}, and covered by 60 nm of polymethylmetacrylate (PMMA) for protection of the nanocrystals ($n \sim 1.5$). A 55 nm silica layer was finally deposited for tuning the Tamm mode at resonance with the nanocrystals' emission. Optical lithography (lift-off resist, 350 nm thickness) was then used to create holes and deposit Ag disks with several microns diameter and 45 nm thickness, which were finally covered by a protective 50 nm layer of PMMA (as in [23], there was no lift-off of the unexposed resist in order to reduce the luminescence from the nanocrystals located outside the disk). The obtained structures are known to exhibit 0D-Tamm states confined between the Bragg mirror and the Ag layer, and localized below the disk [17, 22]. The energy of these states is primarily dependent on the silica+PMMA thickness, with a discretization of these states induced by the lateral confinement for smaller (1–4 μm) disks. For a disk of infinite diameter, transfer matrix simulations find a quality factor close to 200 for these resonant modes.

The fluorescence microscopy setup is shown on figure 1(a). An excitation beam (473 nm, 50 μW pulsed laser) is focused by an objective ($\times$60, 0.7 numerical aperture) onto a $\approx$1 μm spot of the sample. The detected signal is collected by the same objective and sent into an imaging spectrometer. The entrance slit of the spectrometer is conjugated with the Fourier plane of the sample, so that the spectrometer will image the emission spectrum as a function of the emission direction θ_x. The λ–θ_x plot will provide the Tamm state dispersion relation: a 0D-Tamm state with in-plane $k_{x,T}$ wave vector will couple to a photon propagating at an angle $\theta_x = \theta_T$ fulfilling the phase matching condition: $k_{x,T} = (2\pi/\lambda)\sin\theta_T$.

The excitation wavelength is far from the Tamm resonance so that the laser excites directly the nanocrystals which are under the excitation spot. By moving the sample, this excitation spot is chosen at different positions (labeled x_0) on the disk surface. The emission is collected from the whole sample surface, and its wavelength angular dependence will show that it originates from the Tamm states. Our experiment is thus as follows: we probe the emission radiation pattern of the 0D-Tamm states which are excited by the nanocrystals located at position x_0. We will show that the Tamm-state emission properties can be changed by tuning the position of the excited emitters inside the Tamm structure.

Figure 1(b) shows the measured λ–θ_x dispersion relation for various excitation positions x_0 inside a 0D-Tamm disk of diameter 10 μm (similar results, not shown here, were found for a 4 μm disk).

For $x_0 = 0$ (excitation in the center of the disk), the dispersion relation presents the well-known parabolic shape of 2D-Tamm states, starting from a fundamental at $\lambda = 627$ nm (1.98 eV) at $\theta_x = 0$. For all emission wavelengths, the emission radiation pattern is symmetric for θ_x and $-\theta_x$ angles. Thus the measured 0D-Tamm radiation is qualitatively not different from the 2D-Tamm radiation at this point (but differences will appear below for the $x_0 \neq 0$ cases).

When the excitation spot moves away from the disk center ($x_0 \neq 0$), the emission radiation pattern is changed. The λ–θ_x relation remains the same as it corresponds to the 2D-Tamm state dispersion relation, but the light power distribution between left and right is modified. The radiation is then asymmetric and directed mostly into the direction opposite to the position of the excitation spot: $\theta_x > 0$ if $x_0 < 0$ and $\theta_x < 0$ if $x_0 > 0$. We thus have here a form of beaming in the control, by the excitation position, of the radiation pattern asymmetry. This beaming effect is similar to the observations reported in [9–11, 13] for much smaller plasmonic structures, but with a tuning of the excitation position over typical distances of 1 μm instead of 50 nm.

For some positions, we evidence a discretization of the dispersion relation, with a second lobe separated from the lower-energy minimum. This discretization is caused by the boundary conditions introduced by the disk edges. It was not observed for an excitation spot at the center of the disk, due to insufficient mode quality

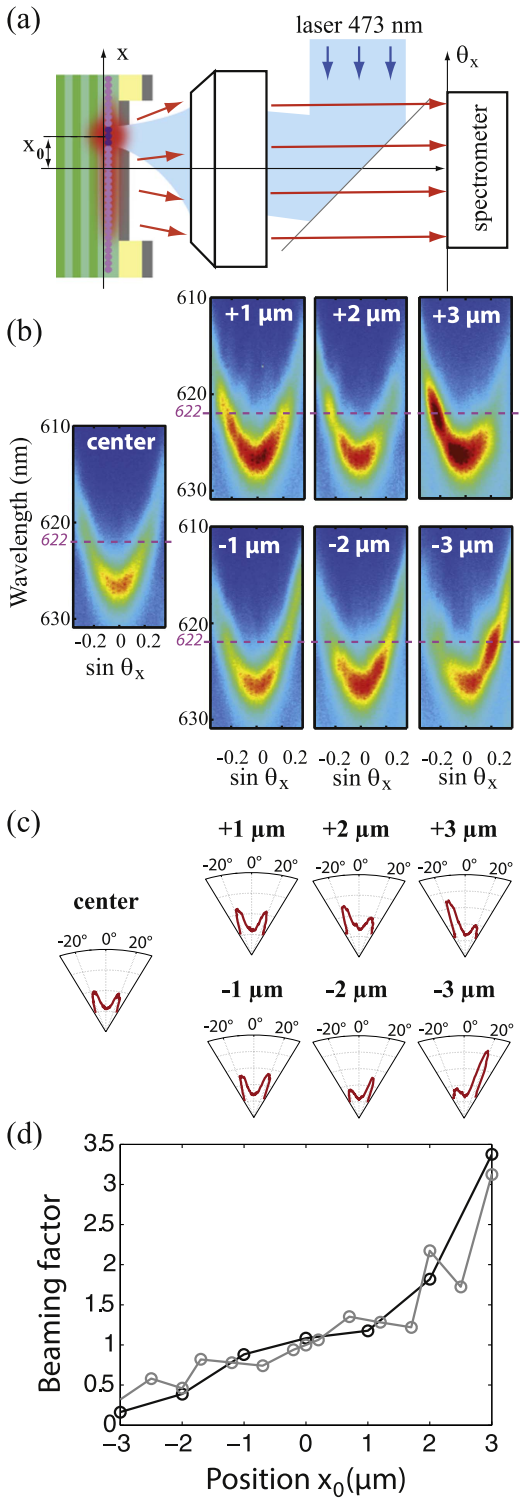

Figure 1. (a) Schematic of the setup; for clarity we omit the lenses in the detection path which conjugate the objective Fourier plane with the entrance plane of the spectrometer; (b) dispersion relations measured for a disk of diameter 10 μm for various excitation positions x_0; (c) corresponding radiation pattern at $\lambda = 622$ nm. (d) Plot of the beaming factor $\zeta = P_-/P_+$, as a function of the source position x_0 (black: experimental; gray: 3D simulation) at 16.5 meV above the fundamental state.

factor, but is revealed by off-centered excitation. Some modes are less excited at given positions because these positions are nodes of those mode's electric field.

Figure 1(c) plots the radiation pattern (detected signal P as a function of θ_x) at a given wavelength $\lambda = 622$ nm ($\Delta E = 16.5$ meV above the fundamental). For all excitation positions x_0, the radiation patterns show 2 lobes around $\pm\theta_T = \pm 18°$, of amplitudes labeled $P_\pm$. The amplitude P_+ (resp. P_-) shows an increase as the excitation position x_0 is shifted downwards (resp. upwards), confirming the beaming effect described above.

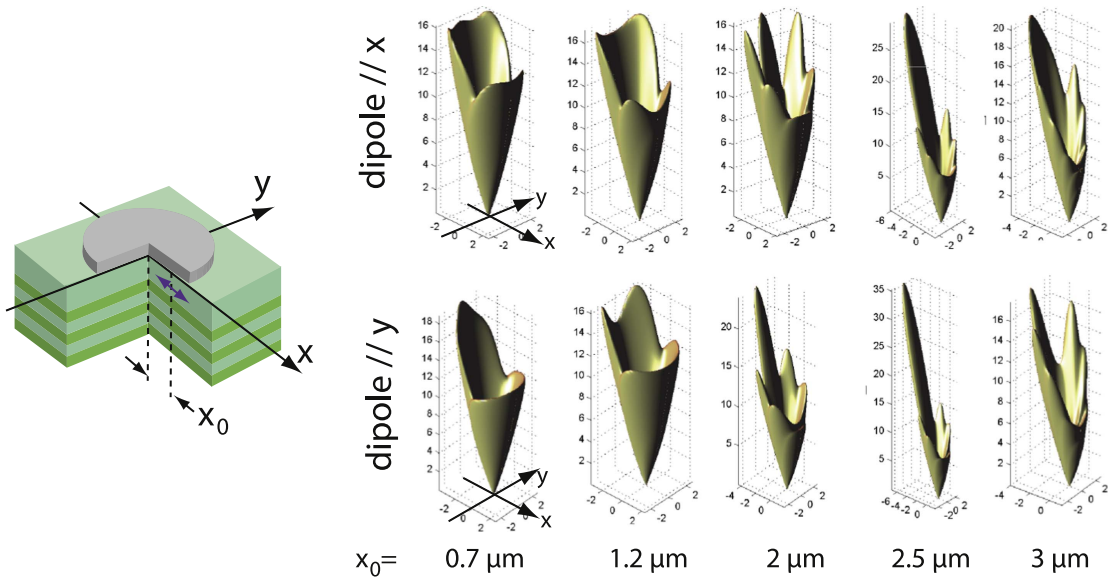

Figure 2. Radiation pattern (angular distribution of emission) calculated for a dipole along x or y direction, located at different positions x_0 along the (Ox) axis, for the same structure geometry as indicated for the experimental Tamm structure (with disk diameter 10 μm and indices: SiO_2 1.45, TiO_2 2.25, Ag 0.055 + 4.25i), at wavelength $\Delta E = 16.5$ meV above the fundamental Tamm state.

If we define a beaming factor ζ as $\zeta = P_-/P_+$, we can plot ζ as a function of x_0 (figure 1(d)). We find then that the beaming factor increases from $\zeta = 1$ at $x_0 = 0$ (no beaming) to $\zeta = 3.4$ at $x_0 = 3$ μm.

These results can be well reproduced by numerical simulations. The 10 μm disk 0D-Tamm structure was simulated by the method described in [24]. Figure 2 shows the resulting radiation patterns calculated for several excitation positions inside the 0D-Tamm disk structure, at an energy $\Delta E = 16.5$ meV above the calculated fundamental. These patterns present a cone shape at an angle θ_T corresponding to the Tamm-state coupling angle, given by the dispersion relation of the 2D-Tamm state. These patterns show clearly the effect of beaming, with the overall emission directed along the direction opposite to the excitation position displacement. As observed experimentally, the beaming becomes stronger as the excitation position is off-centered. This general trend is however combined with the presence of various lobes depending on the excitation position, and also an effect of the excitation dipole orientation (we plot only the x and y orientations on the figure as the z orientation leads to much weaker emission).

The beaming factor $\zeta = P(\theta_x = -\theta_T, \theta_y = 0)/P(\theta_x = \theta_T, \theta_y = 0°)$ which is extracted from the simulations can be superimposed on the experimental data of figure 1(d). There is then a good agreement between measured and calculated beaming factors, confirming that these structures can be used to generate light beaming by tuning the excitation position inside the structure, in a manner which can be simulated *a priori*.

A much-simplified analytical one-dimensional (1D) model can be proposed to highlight the relevant physical phenomena: we consider, at a given frequency, a Tamm state of wave vector $k_T = k' + ik''$ propagating along axis (Ox), confined laterally between $x = -R$ and $x = R$, excited by a dipole at position x_0 (see supplementary information for details; available online at stacks.iop.org/NJP/20/033020/mmedia). The imaginary wave vector component k'' describes the losses of the Tamm states either due to metal absorption, or to coupling with the far-field electromagnetic field. The electric field distribution $E(x)$ can then be determined and its Fourier transform $\hat{E}(k) = \int_{-R}^{R} E(x)e^{-ikx}dx$ corresponds to the radiation pattern of the structure.

Figure 3 shows a typical plot of the radiation pattern $|\hat{E}(k)|^2$ as a function of the radiation angle θ given by $k = (2\pi/\lambda)\sin\theta$, for different positions x_0 and different losses factor k''. As expected, for $x_0 = 0$ (exciting dipole at the center of the structure), the radiation pattern is symmetric. It shows the two expected lobes at angles corresponding to $k = \pm k'$. The width of these lobes increases as a function of the losses factor k''.

As the excitation dipole position x_0 is increased, we find on figure 3 an increase of the peak at $k = -k'$ with respect to the peak at $k = k'$, in agreement with experimental observations. Moreover, we see that the beaming effect, which increases with x_0, increases faster for larger k'' (until the case of very large losses: $k'' = 0.6\ \mu m^{-1} \approx 0.2.k'$: then the beaming effect is less pronounced). For R shorter than the Tamm state losses length ($k'' \ll 1/R$), and for resonant modes ($k' = n\pi/2\ R$), a first-order expansion of our model (see supplementary information) gives:

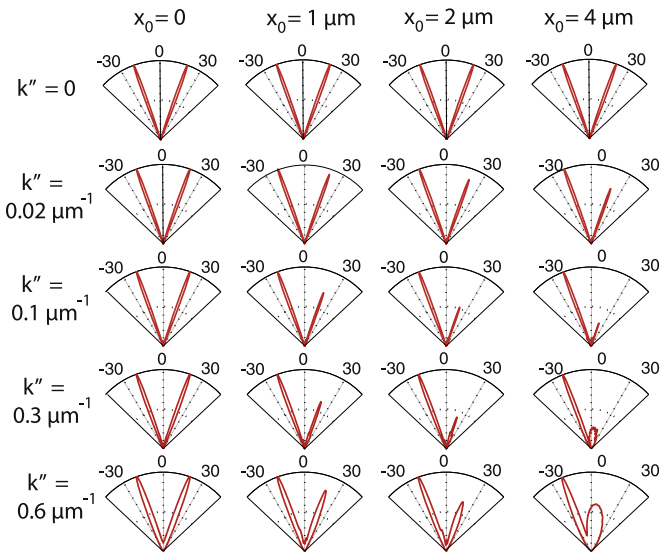

Figure 3. Radiation patterns (normalized to their maximum) calculated by the simplified 1D model with $k' = 3.4\ \mu\text{m}^{-1}$, $\lambda = 620$ nm, $R = 5\ \mu$m and various values of x_0 and k''.

$$\zeta \approx 1 + 4k''x_0$$

which confirms that the beaming effect increases with both x_0 and k''. This first-order expansion agrees reasonably with the curves of figure 3 for the case $k'' = 0.02\ \mu\text{m}^{-1}$ (a fit gives $\zeta = 1.0 + 0.095.x_0$ instead of $1 + 0.08.x_0$) but is not sufficient for the larger values of k''. Now returning to the experimental data of figure 1(c), following this equation we may deduce a propagation length $1/k''$ around 1 μm: however, although of correct order of magnitude, this value is probably largely under-estimated, because of the difference between the 1D model and the actual 3D situation.

Our simplified 1D qualitative model thus suggests that, in order to tune the beaming factor, the position x_0 should be varied over a characteristic length $1/4k''$ corresponding to the typical propagation length of the Tamm state. In the case of the Tamm structure, given the rather low propagation losses of these Tamm states, a good control of ζ is obtained by tuning x_0 with $\sim$1 μm steps. Such position control is easily achieved with optical beams.

In conclusion, we have shown experimentally that 0D-Tamm nanostructures can radiate light into given $\pm\theta_T$ angles. The ratio between the $\pm$ directions (beaming factor ζ) can be controlled, from symmetric emission ($\zeta = 1$) to strong beaming (ζ up to 3.4), by tuning the position of the dipole source in the Tamm structure. The measured beaming factor was found in good quantitative agreement with finite-difference simulations. The Tamm structures thus allow either an active control of beaming by changing the excitation position in a dense layer of source emitters, as was performed here, or the fabrication of structures of controlled beaming by depositing a source emitter at the appropriate position by optical lithography. The required precision for the positioning of the source is of the order of 1 μm, which is easily accessible with optical microscopy. A simplified analytical model suggests that a relevant parameter (characteristic length over which the source position influences beaming) is the attenuation distance of the confined radiating mode.

Acknowledgments

The authors would like to thank Benoît Dubertret and Michel Nasilowski (LPEM) for providing the CdSe/CdS nanocrystals, Jean-Marc Frigerio (INSP), Pascale Senellart (LPN) and Jean-Jacques Greffet (IOGS) for their helpful advice, Willy Daney de Marcillac and Francis Breton (INSP) for their contribution to the microscopy setup, Loïc Becerra and Mélanie Escudier (INSP) for the sample fabrication. This work was supported by the ANR PONIMI (ANR-12-JS04-0011) and the ANR NEHMESIS (ANR-13-BS10-0004).

References

[1] Novotny L 2006 *Principles of Nano-Optics* (Cambridge: Cambridge University Press)
[2] Kim S-H, Kim S-K and Lee Y H 2006 Vertical beaming of wavelength-scale photonic crystal resonators *Phys. Rev.* B **73** 235117
[3] Tran N-V-Q, Combrié S and De Rossi A 2009 Directive emission from high-Q photonic crystal cavities through band folding *Phys. Rev.* **79** 041101(R)

[4] Portalupi S, Galli M, Reardon C, Krauss T F, O'Faolain L, Andreani L C and Gerace D 2010 Planar photonic crystal cavities with far-field optimization for high coupling efficiency and quality factor *Opt. Express* **18** 16064
[5] Yuan X W, Shi L, Wang Q, Chen C Q, Liu X H, Sun L X, Zhang B, Zi J and Lu W 2014 Spontaneous emission modulation of colloidal quantum dots via efficient coupling with hybrid plasmonic photonic crystal *Opt. Express* **22** 23473
[6] Frederich H, Wen F, Laverdant J, Daney de Marcillac W, Schwob C, Coolen L and Maitre A 2014 Determination of the surface plasmon polariton extraction efficiency from a self-assembled plasmonic crystal *Plasmonics* **9** 917
[7] Curto A G, Volpe G, Taminiau T H, Kreuzer M P, Quidant R and van Hulst N F 2010 Unidirectional emission of a quantum dot coupled to a nanoantenna *Science* **329** 930
[8] Belacel C *et al* 2013 Controlling spontaneous emission with plasmonic optical patch antennas *Nano Lett.* **13** 1516
[9] Coenen T, Bernal Arango F, Koenderinck A and Polman A 2014 Directional emission from a single plasmonic scatterer *Nat. Commun.* **5** 3250
[10] Coenen T and Polman A 2014 Optical properties of single plasmonic holes probed with local electron beam excitation *ACS Nano* **8** 7350
[11] Vesseur E and Polman A 2011 Plasmonic whispering gallery cavities as optical nanoantennas *Nano Lett.* **11** 5524
[12] Coenen T, Vesseur E, Polman A and Koenderinck A 2011 Directional emission from plasmonic Yagi-Uda antennas probed by angle-resolved cathodoluminescence spectroscopy *Nano Lett.* **11** 3779
[13] Le Moal E, Marguet S, Rogez B, Mukherjee S, Dos Santos P, Boer-Duchemin E, Comtet G and Dujardin G 2013 An electrically excited nanoscale light source with active angular control of the emitted light *Nano Lett.* **13** 4198
[14] Dousse A, Lanco L, Suffczynski J, Semenova E, Miard A, Lemaitre A, Sagnes I, Roblin C, Bloch J and Senellart P 2008 Controlled light–matter coupling for a single quantum dot embedded in a pillar microcavity using far-field optical lithography *Phys. Rev. Lett.* **101** 267404
[15] Kavokin A V, Shelykh I A and Malpuech G 2005 Lossless interface modes at the boundary between two periodic dielectric structures *Phys. Rev.* B **72** 233102
[16] Kaliteevski M, Iorsh I, Brand S, Abram R A, Chamberlain J M, Kavokin A V and Shelykh I A 2007 Tamm plasmon–polaritons: possible electromagnetic states at the interface of a metal and a dielectric Bragg mirror *Phys. Rev.* B **76** 165415
[17] Gazzano O, Michaelis de Vasconcellos S, Gauthron K, Symonds C, Bloch J, Voisin P, Bellessa J, Lemaitre A and Senellart P 2011 Evidence for confined Tamm plasmon modes under metallic microdisks and application to the control of spontaneous optical emission *Phys. Rev. Lett.* **107** 247402
[18] Braun T, Baumann V, Iff O, Höfling S, Schneider C and Kamp M 2015 Enhanced single photon emission from positioned InP/GaInP quantum dots coupled to a confined Tamm–plasmon mode *Appl. Phys. Lett.* **106** 041113
[19] Gazzano O, Michaelis de Vasconcellos S, Gauthron K, Symonds C, Voisin P, Bellessa J, Lemaitre A and Senellart P 2012 Single photon source using confined Tamm plasmon modes *Appl. Phys. Lett.* **100** 232111
[20] Symonds C, Lheureux G, Hugonin J P, Greffet J J, Laverdant J, Brucoli G, Lemaitre A, Senellart P and Bellessa J 2013 Confined Tamm plasmon lasers *Nano Lett.* **13** 3179
[21] Lheureux G, Azzini S, Symonds C, Senellart P, Lemaître A, Sauvan C, Hugonin J-P, Greffet J-J and Bellessa J 2015 Polarization-controlled confined Tamm plasmon lasers *ACS Photon.* **2** 842
[22] Feng F *et al* 2015 Confined visible optical Tamm states *J. Electron. Mater.* **45** 2307
[23] Feng F *et al* 2016 Spatial and fourier-space distribution of confined optical Tamm modes *New J. Phys.* **18** 083018
[24] Bigourdan F, Hugonin J-P and Lalanne P 2014 Aperiodic Fourier modal method for the analysis of body of revolution photonic structures *J. Opt. Soc. Am.* A **31** 1303